Land subsidence in Xiongan New Area, China revealed by InSAR observations

DAI Keren[1, 2], RAN Peilian[1], LI Zhenhong[3*], AUSTIN Julian[4], MULLER Jan-Peter[5], ZENG Qiming [6], ZHANG Jingfa[7], HU Leyin[8], GOU Jisong[1]

1. *College of Earth Sciences, Chengdu University of Technology, Chengdu* 610059*, China*;
2. *State Key Laboratory of Geohazard Prevention and Geoenviroment Protection, Chengdu University of Technology, Chengdu* 610059*, China*;
3. *COMET, School of Engineering, Newcastle University, Newcastle upon Tyne NE*1 7*RU, UK*;
4. *School of Mathematics, Statistics & Physics, N ewcastle University, Newcastle upon Tyne NE*1 7*RU, UK*;
5. *Mullard Space Science Laboratory, Department of Space & Climate Physics, University College London, Holmbury St Mary RH*5 6*NT, UK*;
6. *School of Earth and Space Sciences, Peking University, Beijing* 100871*, China*;
7. *Key Laboratory of Crustal Dynamics, Institute of Crustal Dynamics, China Earthquake Administration, Beijing* 100085*, China*;
8. *Beijing Earthquake Agency, Beijing* 100080*, China*

Abstract: In 2017, China's central government approved the national strategy to build Xiong'an New Area (XNA, 100 km southwest to Beijing), which was announced as a "millennium strategy" and a "demo area" for a sustainable, modern, and innovative urban model. Xiong'an will draw in as much as $380 billion investment and is expected to help accelerate the development of the wider Beijing-Tianjin-Hebei (Jingjinji) Area. In this paper, present subsidence in the XNA area is investigated using InSAR observations for the first time. The 24 SAR images acquired by European Space Agency's Sentinel-1 satellites during the period from June 2017 to July 2018 suggest that in the north of Xiong County, the subsidence rate reach up to 90 mm/year, which is highly correlated with the exploitation of geothermal drilling. As the construction in the XNA area will significantly accelerate and its high-quality development, the InSAR findings could provide valuable information for future sustainable urban planning and underground infrastructure construction.

Key words: Xiong'an New Area, Subsidence, InSAR, geothermal heating, Sentinel-1

Citation format: Dai K,Ran P L,Li Z H,Austin J L,Muller J P,Zeng Q M,Zhang J F,Hu L Y and Gou J S. 2020. Land subsidence in Xiongan New Area, China revealed by InSAR observations. Journal of Remote Sensing (Chinese). 24(S1): 161-166

1 INTRODUCTION

Xiongan New Area (XNA), established in April 2017, is located about 100 km southwest of Beijing, as a state-level new area in Baoding of Hebei province, China. XNA's development takes place under the direct oversight of the Central Committee of the Communist Party of China and the State Council (Xinhuanet, 2017), which is described as part of the "millennium strategy" and "national strategy". By the middle of the century, it will become a significant part of the world-class Beijing-Tianjin-Hebei (Jingjinji) city cluster, effectively performing Beijing's non-capital functions and providing the Chinese solution to "big city malaise" (The Telegraph, 2018). As the Beijing Plain has suffered from land subsidence for a long time with the subsidence bowl found in Eastern Beijing (Chen et al. 2016), Tianjin (Liu et al., 2016; Zhang et al. 2019), and Langfang (Zhang et al. 2016), evaluation of the subsidence of the XNA area would provide important information and effective support for its long-term urban planning and sustainable development.

Interferometric Synthetic Aperture Radar (InSAR), a unique space-based remote sensing tool to measure the Earth's surface, has been widely used in city subsidence monitoring (Chaussard et al. 2014; Tomás et al. 2014; Dai et al. 2015; Motagh et al. 2017; Chen et al. 2019). Compared to the conventional survey techniques, InSAR features wide coverage, high spatial resolution, high precision and low cost. In previous InSAR studies (Chen et al., 2016; Chen et al., 2019; Ge et al., 2017; Liu et al., 2016; Zhang et al., 2016), it was reported that there was severe subsidence in east of

Received: 2019-10-21; **Accepted:** 2020-04-16

First author biography: DAI Keren (1989—), male, PhD, Professor, his research interests are geohazard evaluation and prevention using InSAR and remote sensing techniques. E-mail: daikeren17@cdut.edu.cn

Corresponding author biography: LI Zhenhong (1975—), male, PhD, Professor, his research interests include earth observations, geohazards, infrastructure stability and precision agriculture. E-mail: Zhenhong.Li@newcastle.ac.uk

Beijing and west of Tianjin, but detailed analysis of the XNA area was absent. Zhang et al. (2018) monitored the ground subsidence in Hengshui to north Tianjin area (including the XNA area) using InSAR techniques with RADARSAT-2 images from 2012—2016, finding that there was subsidence around Xiong county. As the XNA area was officially established in April 2017, a large number of infrastructures will be constructed in the following years. Hence, it is urgent to investigate the present subsidence in the XNA area using InSAR observations.

2 STUDY AREA AND DATA SETS

As shown in Fig. 1, Xiong'an New Area is located in the Hebei Province, North China (marked as a red star in Fig. 1 top left corner inset), about 100 km to Beijing, 100 km to Tianjin and 100 km to Shijiazhuang. The construction of this area was announced to the public out of the blue on April 1, 2017, in which around 100 km^2 was called 'starting zone' in the initial construction and 200 km^2 in the mid-term, 2000 km^2 in the long-term planning. The boundary of Xiong'an New Area is marked with the red polygon in Fig. 1, which covers the contemporary three counties, (namely Xiong county, Rongcheng county and Anxin county) with a total land area of 1560 km^2 and a population of 1.127 million (Jiang et al. 2018). Baoding, Renqiu, Bazhou and Gaobeidian are the nearest cities in the west, south, northeast and north of Xiong'an New Area, respectively. The blue rectangle denotes the coverage of the Sentinel-1 SAR images.

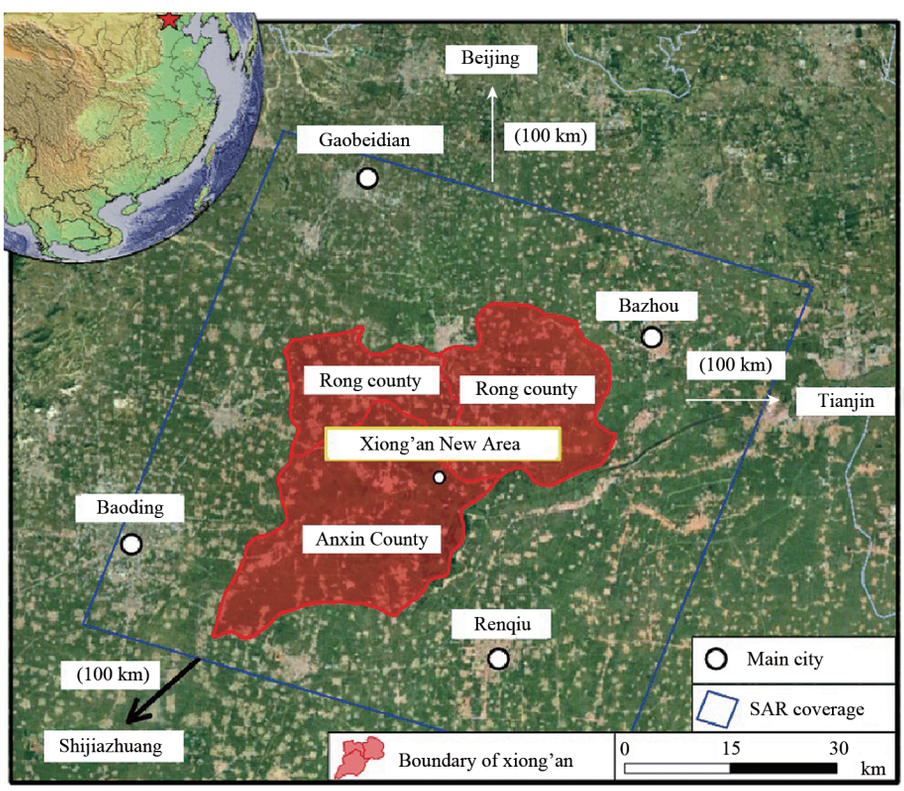

Fig.1 The location of Xiong'an New Area. Note that the blue rectangle indicates the coverage of the descending Sentinel-1 images

To investigate the subsidence of Xiong'an New Area from June 2017 to July 2018, 24 images were acquired by Sentinel-1 satellites, which are conducted by the European Space Agency (ESA) carrying a C-band synthetic aperture radar instrument to provide a collection of data in all-weather, day and night. These images were in the Interferometric Wide swath (IW) TOPS mode with a wavelength of 5.6 cm. The pixel spacing in slant range and azimuth direction of these middle-resolution SAR data are 2.3 m and 13.9 m, respectively. With 167 m and 80 days as the perpendicular baseline and the temporal baseline threshold respectively, in total 85 interferometric pairs were generated to perform the time series InSAR analysis. The detailed acquisition date of each image and interferometric pairs are shown in Fig. 2. The ALOS World 3D (AW3D30) digital surface model (DSM) (JAXA, 2018) was used in this study as the external DEM to remove the topographic contributions in the phase measurements.

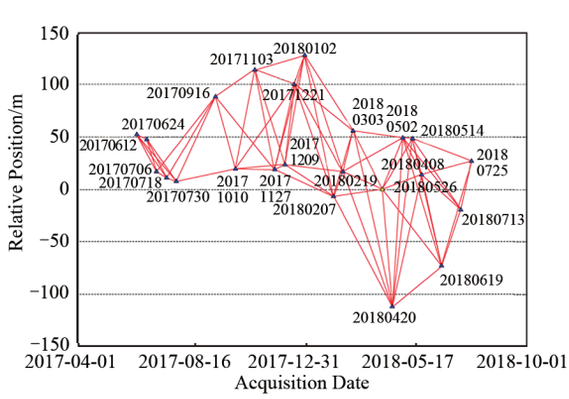

Fig.2 The spatial and temporal baselines of the SAR data sets used in this study

3 METHODOLOGY

A SBAS-InSAR method was used in this study to derive the mean subsidence velocity map and time series subsidence of the XNA area. This method was performed in the ENVI SARscape software and the key steps are presented below.

Assuming *N+1* SLC images covering the area of interests were acquired at the acquistion time $(t_0,t_1,...,t_{n+1})$, one super master image was selected and all the rest of the images were coregistered into the super master image. *M* interferometric pairs were selected and connected according to the given perpendicular baseline and temporal baseline thresholds. Subsequently, with the external DEM, interferometric process was performed including interferogram generation, removal of flat and topographic effects, filtering the interferogram and phase unwrapping with the minimum cost flow (MCF) method.

The interferometric unwrapped phase of an arbitrary pixel *(x,r)* in the j[th] interferogram ($t_b > t_a$), i.e. $\delta\phi^j(x,r)$, can be written as,

$$\delta\phi^j(x,r) = \phi^j_{def}(x,r) + \phi^j_{topo}(x,r) + \phi^j_{atm}(x,r) + \phi^j_{noise}(x,r) = \frac{4\pi}{\lambda}\left[d(t_B,x,r) - d(t_A,x,r)\right] + \frac{B\perp\Delta z}{r\sin\theta} + \Delta d_{atm} + \Delta n \quad (1)$$

where λ denotes the radar wavelength; $d(t_B,x,r)$and $d(t_A,x,r)$ are the accumulated displacement in the radar line of sight (LOS) direction; $\phi^j_{topo}(x,r)$ accounts for the topographic residue with respect to the perpendicular baseline $B_\perp$ and the elevation differenceΔ_Z; Δd_{atm} denotes atmospheric artifacts; Δ_n is decorrelation noise. Δd_{atm} and Δ_n can be separated from the interferometric phase by a high-pass filter in the time domain and low-pass filter in the spatial domain (Goldstein et al. 1995).

The $\phi^j_{def}(x,r)$ in Eq. (1) could be expressed with the mean phase velocity between time adjacent acquisitions as,

$$v^T = \left[v_1 = \frac{\phi_1}{t_1 - t_0},...,v_N = \frac{\phi_N - \phi_{N-1}}{t_N - t_{N-1}}\right] \quad (2)$$

Therefore, the unwrapped interferometric phase $\delta\phi^j(x,r)$ is only related to $\phi^j_{def}(x,r)$ and $\phi^j_{topo}(x,r)$, expressed as,

$$\delta\phi^j(x,r) = \sum_{k=t_{Aj}}^{t_{Bj}}(t_k - t_{k-1}).v_k + \frac{B\perp\Delta z}{r\sin\theta} \quad (3)$$

Combining *M* unwrapped differential interferograms for pixel *(x,r)* into equations (1), (2) and (3), *N* unknown deformation rates and the topographic error *Z(x,r)* can be solved in a least squares sense (If all the acquisitions are well connected, we should have an overdetermined system, i.e. $M > N+1$). This calculation was included in the first inversion. After the re-unwrapping step to correct some interferograms, the second inversion was performed to remove atmospheric artifacts again. As a result, the refined average displacement rate, time series displacement and topographic correction were acquired. The whole flowchart is shown in Fig. 3 and more details can be found in Guo et al. (2017).

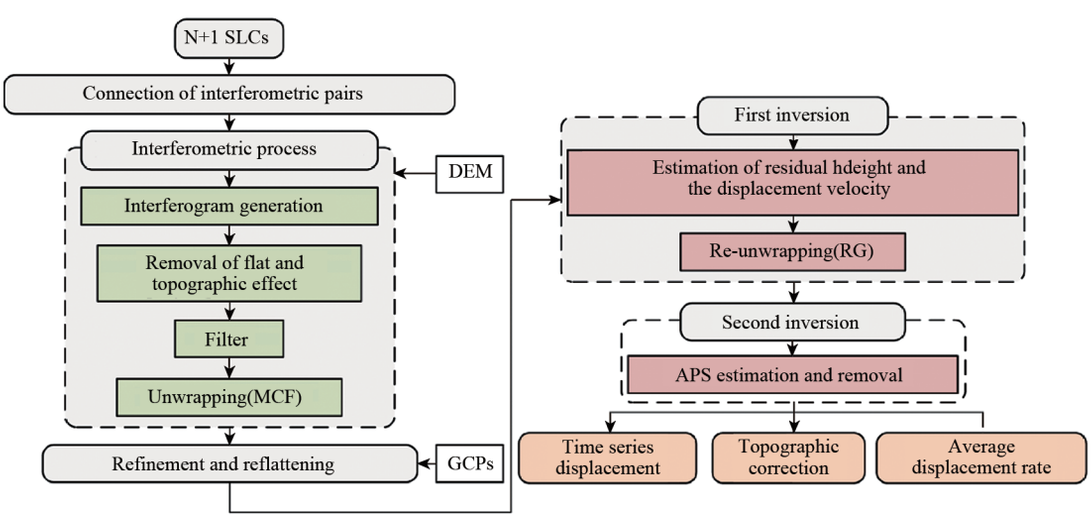

Fig.3 Flowchart of the SBAS InSAR method

4 RESULTS AND ANALYSIS

4.1 Mean velocity and time series displacement

The mean subsidence velocity was derived by the SBAS InSAR method based on the Sentinel-1 images from June 2017 to July 2018. It is clear in Fig. 4 that two obvious subsidence zones can be observed, marked by white dotted lines. One is on the south of Xiongan New Area, covering Gaoyang County (i.e. Zone b), with a maximum subsidence rate of 90 mm/year. The width of this subsidence zone is more than 25 km and the north boundary of this subsidence is very close to Anxin County. The second subsidence one is in the north of Xiong county with a maximum rate of 90 mm/year (i.e. Zone a), which is long and narrow (about 30 km long and 5 km wide). The affected area reaches 150 km^2, which accounts for 28.6% of the whole Xiong County area. In Rong County and most of Anxin County, no obvious subsidence is observed, suggesting the ground is stable.

In order to analyze the temporal subsidence in the subsidence zones, 10 points are selected to extract their corresponding displacement time series during the period from June 2017 to July 2018, whose locations are shown in Fig. 4 (i.e. points 1—10). The displacement time series of these points are shown in Fig. 5. It can be seen that the subsidence on all these points exhibit a linear trend. In the subsidence zone a, in the north of Xiong County, points #4 and #5 are in the subsidence center and their accumulated displacements reach up to 85—90 mm. Points #1,#2 and #3 are

relatively a little further away from the subsidence center with accumulated displacements of 30—50 mm. In the subsidence zone b, points #7 and #8 present a maximum accumulation displacement of 90—95 mm. Points #6 and #9 are close to the boundary of Anxin County, on which the accumulated displacements decreases to 40—65 mm. Point #10 is in the middle between Gaoyang County and Renqiu city with an accumulation displacement of 30 mm.

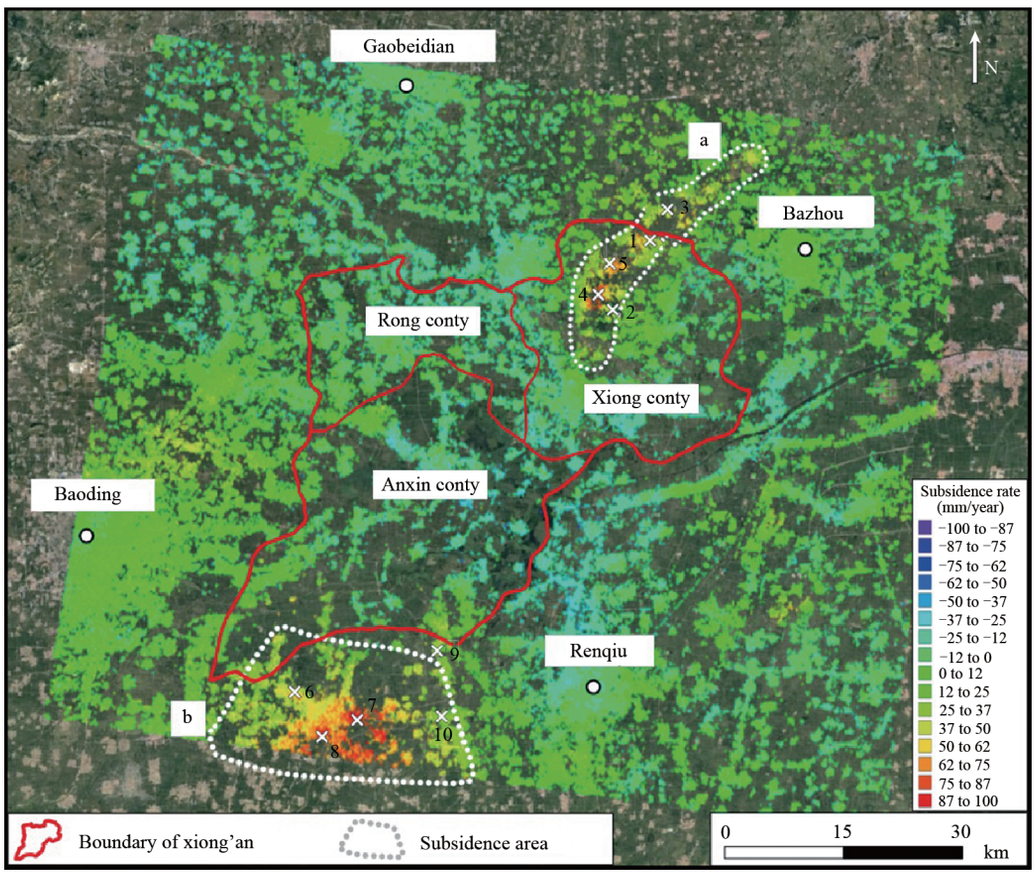

Fig.4 Mean subsidence velocity covering Xiong'an New Area

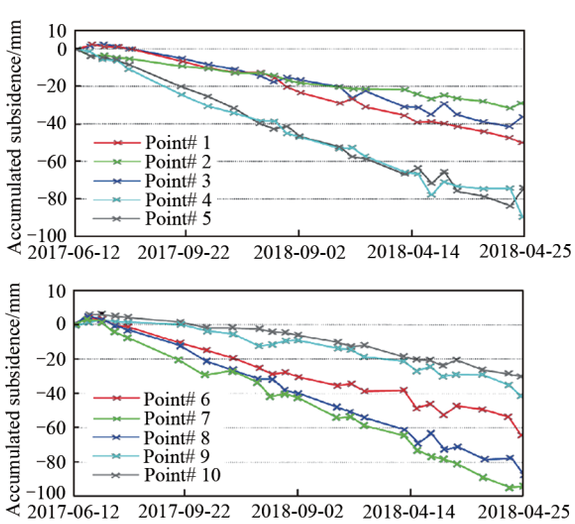

Fig.5 Displacement time series for Points #1−10 whose locations are shown in Fig. 4

4.2 Analysis on detailed subsidence with geothermal exploitation

XNA has rich geothermal resources in the shallow layer, up to 200 meters deep, which may provide more easily accessible sources of heat for the wide area (Ecns.cn 2017). Xiong County has achieved overall geothermal coverage for heating purposes and become the first "Smoke-free City" across the country (Wang et al. 2018). In 2003, some residents began to use geothermal resources for heating. In 2009, a state-owned enterprise boosted the project of using geothermal heat instead of coal firing. As a result, the area using geothermal heating increases by several hundred thousand square meters per year in Xiong county, which has reached up to 4.47 million square meters (China.com, 2017). In Xiong county, geothermal resources from Karst reservoirs are being developed for space heating to a very large scale, up to 4.5 million m^2 using hot water from a single geothermal field, the largest in the world, and the coverage of space heating in the county is 95% by geothermal (Pang et al. 2018).

Land subsidence is one of the potential risks of geothermal exploitation, which has been observed in some cases (The Telegraphy, 2008; Allis et al. 2009). In order to exploit the relationship between the subsidence and geothermal drilling in Xiong County, the subsidence map and the distribution of geothermal wells are overlaid in Fig. 6a. It should be noted that the geothermal well data was extracted in 2009 (adapted from Pang, 2011), but the current distribution of geothermal wells would be much denser due to the rapid development in Xiong county in the last decade. It can be seen that all of the geothermal wells were distributed mainly in three zones, in the southwest of Xiong County downtown, in the downtown

center of Xiong County and in the north of Xiong County downtown (blue area in Fig. 6(a)). There is no subsidence found in the former two zones. In the north of Xiong County downtown, the severe subsidence with a maximum rate of 95 mm/year occurred, where there are a large number of geothermal wells. It is clear that this narrow and long subsidence area (red area in Fig. 6(a)) has a high correlation with the distribution of the geothermal wells (blue area in Fig. 6(a)). In addition, due to the deep store of geothermal resources and high economic and technological requirements for utilization, the east of Xiong County is not suitable for geothermal exploitation (Pang, 2011) and there is no subsidence found. These findings may provide significant reference for the long-time planning of the geothermal and underground exploitation in the XNA area.

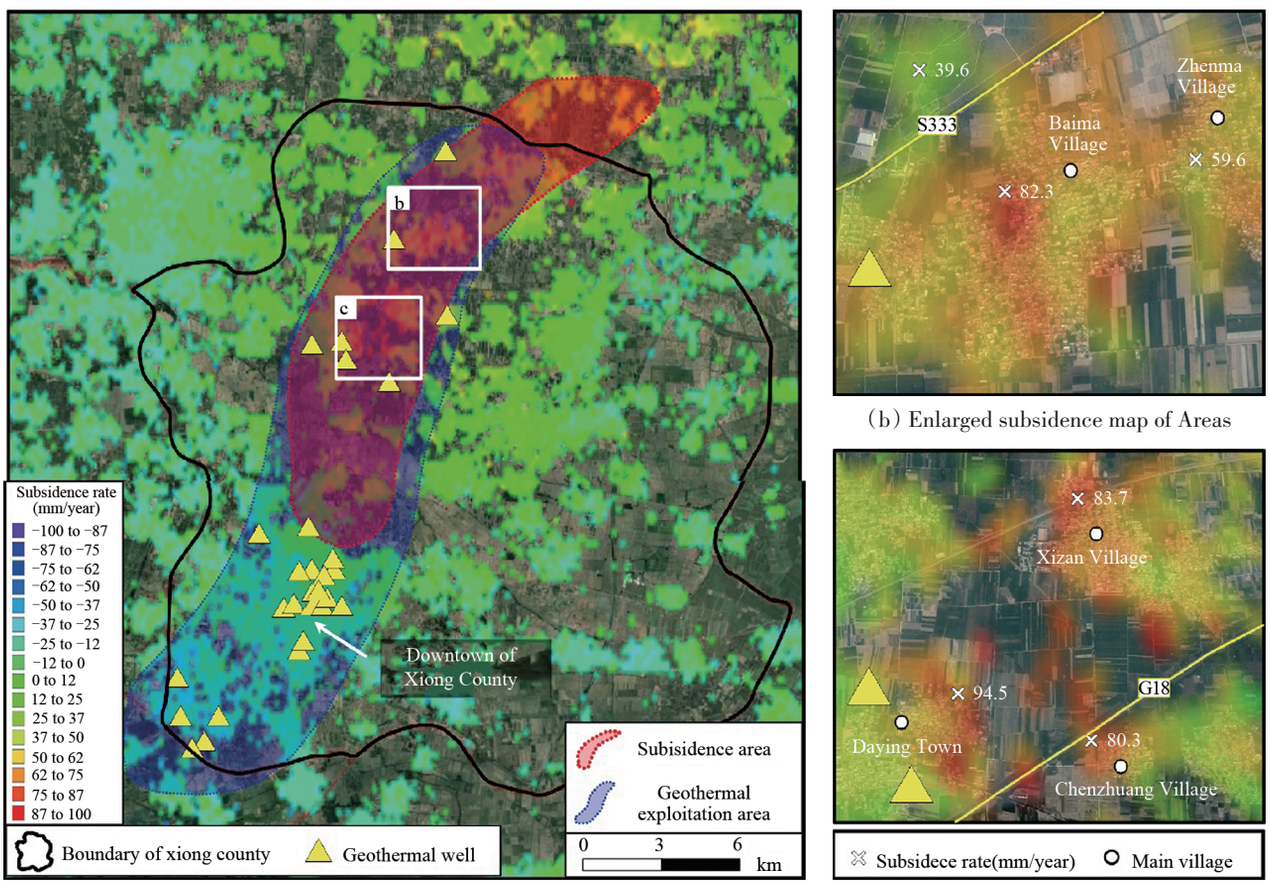

(a) Subsidence map in Xiong County with the distribution of geothermal wells (indicated by yellow triangles)

(b) Enlarged subsidence map of Areas

(c) Large villages

Fig.6 The enlarged subsidence map in Xiong County

Two severe subsidence zones occurred in the north of the Xiong County downtown and they were presented in detail. In Fig. 6b, the maximum subsidence occurred with a rate of 82 mm/year in Baima village, which is close to the Hebei Provincial Road S333. Zhenma village is in the east of Baima village and the subsidence rate decreases to 60 mm/year. In the north of S333, the subsidence has weakened with a rate of 39 mm/year. As shown in Fig. 6c, the maximum subsidence also occurred in Daying town and Xizan village in the north of G18 RongWu highway, with a rate of 94.5 mm/year and 83.7 mm/year, respectively. In Chenzhuang Village, at the north of G18, the subsidence rate reaches to 80.3 mm/year. All of these villages need special attention on the construction and geothermal exploitation in the future development.

5 CONCLUSIONS

In this paper, the subsidence in the XNA area has been investigated using 24 scenes of ESA's Sentinel-1 SAR images acquired from June 2017 to July 2018. InSAR time series results suggest that there are two subsidence zones in the XNA area: one on the south of Anxin County and the other in the north of Xiong County with a maximum subsidence rate of 95 mm/year. The subsidence area in Xiong County has a length of 30 km, affecting 150 km^2, accounting for 28.6% of the whole Xiong County area. According to the time series result, these two subsidence zones exhibit a linear trend during 2017—2018.

In addition, as Xiong County has rich geothermal resources and the geothermal exploitation has dramatically accelerated since 2009, the relationship between subsidence and the distribution of geothermal wells has been analyzed. It was found that in the north of Xiong County, the subsidence has a strong correlation with the distribution of geothermal wells. It is speculated that geothermal drilling would have an effect on the subsidence to some degree in Xiong County. Detailed analyses on this area reveal that severe subsidence has occurred in Xizan Village, Baima Village, Chenzhuang Village and Daying Town. These findings are believed to provide valuable information for future urban planning and underground infrastructure construction.

REFERENCES

Allis R, Bromley C and Currie S, 2009. Update on subsidence at the Wairakei – Tauhara geothermal system, New Zealand. Geothermics, 38(1), 169-180.

Chen B, Gong H, Lei K, Li J, Zhou C, Gao M, Guan H and Lv W, 2019. Land subsidence lagging quantification in the main exploration aquifer layers in Beijing plain, China. International Journal of Applied Earth Observation and Geoinformation, 75, 54-67.

Chen M, Tomás R, Li Z, Motagh M, Li T, Hu L, Gong H, Li X, Yu J and Gong X, 2016. Imaging land subsidence induced by groundwater extraction in beijing (china) using satellite radar interferometry. Remote Sensing 8: 468.

Chaussard E, Wdowinski S, Cabral-Cano E and Amelung F, 2014. Land subsidence in central Mexico detected by ALOS InSAR time-series. Remote sensing of environment, 140, 94-106.

China.com, 2017. Xiong County: rich in geothermal resources and geothermal heating began 14 year ago, https://news.china.com/domesticgd/10000159/20170415/30422814.html

Dai K, Liu G, Li Z, Li T, Yu B, Wang X and Singleton A, 2015. Extracting vertical displacement rates in shanghai (china) with multi-platform sar images. Remote Sensing 7: 9542-9562. doi: 10.3390/rs70809542

Ecns. cn, 2017. Xiongan looks good in survey, https://www. ecns. cn/2017/08-24/270632.shtml

Ge D, Zhang L, Wang Y, Li M, Liu B, Guo X, Wang Y, 2017. Interferometric synthetic aperture radar: detect detail from faraway place. Scientific and Cultural Popularization of Land and Resources.

Goldstein R, 1995. Atmospheric limitations to repeat-track radar interferometry. Geophysical Research Letters. 22(18), 2517 – 2520

Guo J, Hu J, Li B, Zhou L and Wang W, 2017. Land subsidence in Tianjin for 2015 to 2016 revealed by the analysis of Sentinel-1A with SBAS-InSAR. Journal of Applied Remote Sensing, 11(2), 026024.

JAXA,2018. ALOS Global Digital Surface Model "ALOS World 3D - 30m (AW3D30)". https://www. eorc. jaxa. jp/ALOS/en/aw3d30/index.htm

Jiang L, Lv P, Feng Z, Liu Y, 2018. Where Should the Start Zone Be Located for Xiong'an New Area? A Land Use Perspective. Journal of Resources and Ecology, 9(4), 374-382.

Liu P., LiQ., LiZ., HoeyT., LiuG., WangC., HuZ., ZhouZ., and SingletonA., 2016. Anatomy of Subsidence in Tianjin from Time Series InSAR, Remote Sensing, 8(3), 266.

Motagh M, Shamshiri R, Haghighi M, Wetzel H, Akbari B, Nahavandchi H, Roessner S and Arabi S, 2017. Quantifying groundwater exploitation induced subsidence in the Rafsanjan plain, southeastern Iran, using InSAR time-series and in situ measurements. Engineering Geology, 218, 134-151.

TelegraphThe, 2008. Geothermal probe sinks German city, https://www. telegraph.co.uk / news / worldnews / 1583323 / Geothermal - probe-sinks- German-city.html

TelegraphThe, 2018. Highlights of xiongan new area master plan. https: //www. telegraph. co. uk/news/world/china-watch/business/highlights-of-xiongan-development/

Tomás R, Romero R, Mulas J, Marturià J, Mallorquí J, Lopez-Sanchez, J, Herrera G, Gutierrez F, Gonzalez P, Fernandez J, Duque S, Concha-Dimas A, Cocksley G, Castaneda C, Carrasco D, Blanco P, 2014. Radar interferometry techniques for the study of ground subsidence phenomena: a review of practical issues through cases in Spain. Environmental earth sciences, 71(1), 163-181.

Pang Z, Kong Y, Shao H and Kolditz O, 2018. Progress and perspectives of geothermal energy studies in China: from shallow to deep systems.

Pang J, 2011. A geothermal sustainable development study based on assessment of mining conditions and reinjection potential: a case study of Xiongxian County, Hebei province. Master thesis, Capital Normal University.

Wang S, Liu J, Sun Y, Liu S, Gao X, Sun C, Li H, 2018. Study on the geothermal production and reinjection mode in Xiong County. Journal of Groundwater Science and Engineering, 6(3), 178-186.

Wang Z, Jiang G, Zhang C, Hu J, Shi Y, Wang Y, and Hu S, 2018. Thermal regime of the lithosphere and geothermal potential in Xiong'an New Area. Energy Exploration & Exploitation, 0144598718778163.

Xinhuanet, 2017. China to create xiongan new area in hebei. http:// www.xinhuanet.com//english/2017-04/01/c_136177270.htm

Zhang X, 2018. Analysis and stratages on the prevention of ground subsidence for Xiong'an New Area development. Chinese Engineering Consulting, 04: 10-15.

Zhang T, Shen W, Wu W, Zhang B, and Pan Y, 2019. Recent Surface Deformation in the Tianjin Area Revealed by Sentinel-1A Data. Remote Sensing, 11(2), 130.

Zhang Y, Liu B, Wu H, Cheng X, Kang Y, 2018. Ground subsidence in Xiong'an New Area from 2012 to 2016 monitored by InSAR Technique. Journal of Earth Sciences and Environment, 40(5), 652-662.

Zhang Y, Wu H, Kang Y, 2016. Ground subsidence over Beijing-Tianjin-Hebei region during three periods of 1992 to 2014 monitored by interferometric SAR. Acta Geodaetica et Cartographica Sinica, 45(9): 1050-1058.

Zhang Y, Wu H, Kang Y, and Zhu C, 2016. Ground subsidence in the Beijing-Tianjin-Hebei region from 1992 to 2014 revealed by multiple sar stacks. Remote Sensing, 8(8), 675.